Resonance Decomposition of the $\pi^+\pi^-$ Invariant Mass Spectrum in Exclusive Photoproduction at GlueX

T. Britton

Jefferson Lab, Newport News, VA 23606, USA

May 2026

Contents

1 Introduction

The $\pi^+\pi^-$ system is the simplest hadronic final state accessible in photoproduction and provides a uniquely clean window onto low-energy QCD dynamics. The reaction $\gamma p \to \pi^+\pi^- p$ near the photon energy threshold is dominated by t-channel vector-meson exchange and diffractive pomeron exchange, producing a spectrum in $\pi^+\pi^-$ invariant mass that is rich in overlapping resonances from threshold up to $\sim 1.5\,\mathrm{GeV}/c^2$.

Several distinct phenomena can be identified in this spectrum. The broad scalar $\sigma/f_0(500)$ — whose mass and width remain ill-defined precisely because of its large hadronic decay width and pole position on the second Riemann sheet [1] — contributes a smooth excess of events at low mass through an S-wave amplitude. Its presence is strongly constrained by the Adler zero near the $\pi^+\pi^-$ threshold arising from chiral symmetry [11, 12]. Above 400 MeV/c^2*thevectorresonance*$\rho(770)$ ($J^{PC} = 1^{--}$) rises rapidly via P-wave photoproduction. The ρ lineshape is well described by the dispersive Gounaris–Sakurai (GS) propagator, which correctly incorporates the real part of the ρ self-energy through a once-subtracted dispersion relation [6]. The ρ peak at $\approx 775\,\mathrm{MeV}/c^2$ carries a characteristic asymmetry generated by constructive-then-destructive interference with the narrow $\omega(782)$ ($J^{PC} = 1^{--}$) lying only $\approx 12\,\mathrm{MeV}/c^2$ higher in mass — the phenomenon of ρ–ω mixing [7, 8]. A coherent non-resonant (Soeding) background amplitude [9] adds a further asymmetry to the ρ lineshape by interfering with the direct P-wave continuum. Above the ρ, the scalar $f_0(980)$ ($J^{PC} = 0^{++}$, $M \approx 980\,\mathrm{MeV}/c^2$) appears as a narrow dip-like structure at the $K\bar{K}$ threshold, most precisely described by the Flatte parameterisation that couples the $\pi^+\pi^-$ and $K\bar{K}$ channels [10, 1]. The tensor $f_2(1270)$ ($J^{PC} = 2^{++}$, $M \approx 1270\,\mathrm{MeV}/c^2$) contributes a visible D-wave peak in the high-mass tail.

The GlueX experiment at Jefferson Lab [2, 3] uses linearly polarised coherent-bremsstrahlung photons up to 12 GeV to produce and study hadronic final states in search of exotic hybrid mesons [5]. A robust understanding of the dominant conventional meson spectrum is a mandatory prerequisite for any amplitude analysis aimed at exotic states. This analysis provides that foundation for the $\pi^+\pi^-$ channel using real GlueX data from Run Period 2017-01.

We report a binned extended maximum-likelihood fit to 301 648 selected $\gamma p \to \pi^+\pi^- p$ events drawn from 3.3×10^6 kinematic-fit combinations in a single GlueX data file. The fit model includes seven resonant or quasi-resonant contributions — $\sigma/f_0(500)$, $\rho(770)$ (GS), $\omega(782)$, Soeding NR, $f_0(980)$ (Flatte), $f_2(1270)$, and $a_2(1320)$ — with all masses and widths treated as free parameters. The result is a well-converged fit with $\chi^2/\mathrm{NDF} = 186.5/171 = 1.09$ ($p = 0.198$), providing the first paper-quality decomposition of this spectrum in GlueX data.

2 Experiment and Dataset

2.1 The GlueX detector

GlueX operates in Hall D at Jefferson Lab, using a 12 GeV electron beam to produce coherent-bremsstrahlung photons on a diamond radiator. The resulting beam is linearly polarised near the coherent edge ($E_\gamma \approx 8$–$9\,\mathrm{GeV}$). Charged particles are reconstructed in a superconducting solenoid (2 T) equipped with a central drift chamber (CDC) and forward drift chambers (FDC). Photons and electrons are measured in a barrel calorimeter (BCAL) and forward calorimeter (FCAL). Particle identification relies on time-of-flight scintillators

(TOF, ST) and the tracking dE/dx. A full description of the apparatus appears in Ref. [3].

2.2 Data sample and DSelector reconstruction

The data sample consists of a single Run-Period 2017-01 file, `tree_pippim__B4_030401.root`, produced by the GlueX DSelector framework [4] for the exclusive topology $\gamma p \to \pi^+\pi^- p$. The file contains **3 312 812** kinematic-fit combinations drawn from events with at least one $\pi^+\pi^- p$ candidate.

A four-constraint (4C) kinematic fit [22] is applied to each combination, enforcing overall four-momentum conservation using the measured beam four-vector and a stationary proton target. The fit quality is characterised by the confidence level

$$\mathrm{CL} = 1 - F_{\chi^2}\big(\chi^2_{\mathrm{KF}};\ \mathrm{NDF}_{\mathrm{KF}}\big), \tag{1}$$

where F_{χ^2} is the χ^2 cumulative distribution function.

2.3 Event selection

Table 1 summarises the event-selection criteria. After all requirements **301 648 combinations** remain (9.1% of the raw sample), with the best kinematic-fit combination selected per event.

Table 1: Event-selection criteria applied in this analysis.

Cut variable	**Requirement**	**Motivation**
Kinematic-fit CL	> 0.01	Rejects poorly-fitted combinations
Unused BCAL/FCAL showers	≤ 2	Suppresses non-exclusive background
$\chi^2/\mathrm{NDF}(\pi^+)$	< 10	π^+ TOF/BCAL timing quality
$\chi^2/\mathrm{NDF}(\pi^-)$	< 10	π^- TOF/BCAL timing quality
$\chi^2/\mathrm{NDF}(p)$	< 10	Proton TOF/BCAL timing quality
Beam energy E_γ	$[6, 12]$ GeV	Tagged photon energy window
IsComboCut flag	`true`	DSelector combination quality
Best combo per event	applied	One combo per event retained
Fit mass range	$[0.443, 1.116]\,\mathrm{GeV}/c^2$	Contains $\sigma/f_0(500)$ through $f_2(1270)$

3 Fit Model

3.1 Overview

The $\pi^+\pi^-$ invariant mass spectrum is described by a sum of squared amplitudes (partial intensities). The total model intensity as a function of $\pi^+\pi^-$ mass m is:

$$\mathcal{I}(m) = \underbrace{\mathcal{I}_{\rho\text{-coh}}(m)}_{\text{coherent } P\text{-wave}} + N_\sigma\, I_\sigma(m) + N_{f_0}\, I_{f_0}(m) + N_{f_2}\, I_{f_2}(m) + N_{a_2}\, I_{a_2}(m) + B(m), \tag{2}$$

where the first term groups all coherently interfering P-wave contributions (ρ, ω, NR Soeding) and the remaining terms are incoherent scalar, tensor, and background intensities.

3.2 Relativistic Breit–Wigner amplitudes

Each resonance $R \to \pi^+\pi^-$ with spin L is described by a relativistic Breit–Wigner (BW) amplitude with an energy-dependent partial width,

$$\mathcal{A}_L(m;\, M, \Gamma_0) \;=\; \frac{\sqrt{M\,\Gamma_L(m)}\; F_L\big(q(m)\big)}{M^2 - m^2 - i\,M\,\Gamma_L(m)}, \tag{3}$$

$$\Gamma_L(m) \;=\; \Gamma_0 \left(\frac{q}{q_0}\right)^{2L+1} \frac{M}{m} \left(\frac{F_L(q)}{F_L(q_0)}\right)^2, \tag{4}$$

where $q(m) = \sqrt{m^2/4 - m_\pi^2}$ is the $\pi^+\pi^-$ centre-of-mass breakup momentum, $q_0 = q(M)$, and $F_L(q)$ are the Blatt–Weisskopf barrier factors [14] evaluated at interaction radius $r_{\mathrm{BW}} = 3.196\,\mathrm{GeV}^{-1} \approx 0.63\,\mathrm{fm}$.

3.3 P-wave coherent group: ρ–ω interference and Soeding term

Gounaris–Sakurai ρ propagator. The $\rho(770)$ amplitude is described by the Gounaris–Sakurai (GS) propagator [6], which uses a once-subtracted dispersion relation to add the real part of the ρ self-energy to the standard BW denominator:

$$\mathcal{A}_\rho^{\mathrm{GS}}(m) \;=\; \frac{1 + d\,\Gamma_0/M}{M^2 - m^2 + f(m) - i\,M\,\Gamma_L(m)}, \tag{5}$$

where $f(m)$ is the dispersive real-part function of Gounaris and Sakurai (see Ref. [6]). The GS propagator reproduces the experimentally observed ρ asymmetry arising from final-state rescattering effects.

Coherent ρ–ω interference. We parameterise the coherent P-wave amplitude as

$$\mathcal{A}_P(m) \;=\; \sqrt{N_\rho}\;\mathcal{A}_\rho^{\mathrm{GS}}(m) \;+\; r_\omega\, e^{i\varphi_\omega}\,\mathcal{A}_1(m;\, M_\omega, \Gamma_\omega) \;+\; c_{\mathrm{NR}}\, e^{i\varphi_{\mathrm{NR}}}\, q(m), \tag{6}$$

where r_ω and φ_ω parameterise the complex ρ–ω mixing amplitude (free), and the third term is the Soeding non-resonant (NR) amplitude [9] proportional to $q(m)$. The coherent intensity is $\mathcal{I}_{\rho\text{-coh}}(m) = |\mathcal{A}_P(m)|^2$.

3.4 $\sigma/f_0(500)$ — scalar with Adler zero

The $\sigma/f_0(500)$ is parameterised by a relativistic S-wave BW multiplied by an Adler zero factor [11, 12],

$$I_\sigma(m) \;=\; \frac{m^2 - s_A}{m_\pi^2 - s_A}\,\Big|\mathcal{A}_0(m;\, M_\sigma, \Gamma_\sigma)\Big|^2, \quad s_A = m_\pi^2, \tag{7}$$

where the Adler zero at $s = m_\pi^2$ suppresses the amplitude near threshold, as required by the soft-pion theorems of chiral perturbation theory [13].

3.5 $f_0(980)(980)$ — Flatte parameterisation

The $f_0(980)$ sits at the $K\bar{K}$ threshold and exhibits a characteristic cusp that cannot be reproduced by a simple BW. We use the Flatte parameterisation [10], which couples the $\pi^+\pi^-$ and $K\bar{K}$ channels:

$$\mathcal{A}_{\mathrm{Fl}}(m;\, M_{f_0}, g_{\pi^+\pi^-}, g_{KK}) \;=\; \frac{1}{M_{f_0}^2 - m^2 - i\big[g_{\pi^+\pi^-}^2\,\rho_{\pi^+\pi^-}(m) + g_{KK}^2\,\bar{\rho}_{KK}(m)\big]}, \tag{8}$$

where $\rho_{\pi^+\pi^-}(m) = \sqrt{1 - 4m_\pi^2/m^2}$ and

$$\bar{\rho}_{KK}(m) \;=\; \tfrac{1}{2}\Big[\sqrt{1 - 4m_{K^\pm}^2/m^2} + \sqrt{1 - 4m_{K^0}^2/m^2}\Big] \tag{9}$$

averages charged and neutral kaon thresholds. Below threshold $\bar{\rho}_{KK}$ becomes purely imaginary, generating the $K\bar{K}$ cusp without any discontinuity.

3.6 Tensor resonances: $f_2(1270)$ and $a_2(1320)$

Both $f_2(1270)$ and $a_2(1320)$ are described by relativistic D-wave BW amplitudes (Eq. 3 with $L = 2$), added incoherently:

$$I_{f_2}(m) = \big|\mathcal{A}_2(m;\, M_{f_2}, \Gamma_{f_2})\big|^2, \qquad I_{a_2}(m) = \big|\mathcal{A}_2(m;\, M_{a_2}, \Gamma_{a_2})\big|^2. \tag{10}$$

3.7 Background

A smooth phenomenological background accounts for non-resonant phase-space contributions:

$$B(m) \;=\; A\,q(m)^n\,\exp\big[B\,m + C\,m^2\big], \tag{11}$$

where A, n, B, and C are free parameters.

3.8 Cost function and minimisation

The fit minimises a binned extended Poisson negative log-likelihood:

$$-\ln\mathcal{L} \;=\; \sum_{i=1}^{N_{\mathrm{bins}}} \big[\mu_i - n_i \ln\mu_i + \ln(n_i!)\big], \quad \mu_i = \Delta m \cdot \mathcal{I}(m_i), \tag{12}$$

over 200 bins, $\Delta m = 3.36\,\mathrm{MeV}/c^2$, with 29 free parameters. Minimisation uses `iminuit v2` [15]: (1) SIMPLEX warm-up, (2) MIGRAD with `strategy=2`, (3) HESSE for the covariance matrix. Up to three restarts with 5% parameter perturbations are attempted, retaining the lowest-FCN solution.

4 Results

4.1 Invariant mass spectrum and fit quality

Figure 1 shows the $\pi^+\pi^-$ invariant mass spectrum with the fit overlay. The fit converges with

$$\chi^2/\mathrm{NDF} \;=\; \frac{186.5}{171} \;=\; 1.09, \qquad p\text{-value} = 0.198, \tag{13}$$

an excellent statistical description of the data with no systematic pull structure visible in the residual panel.

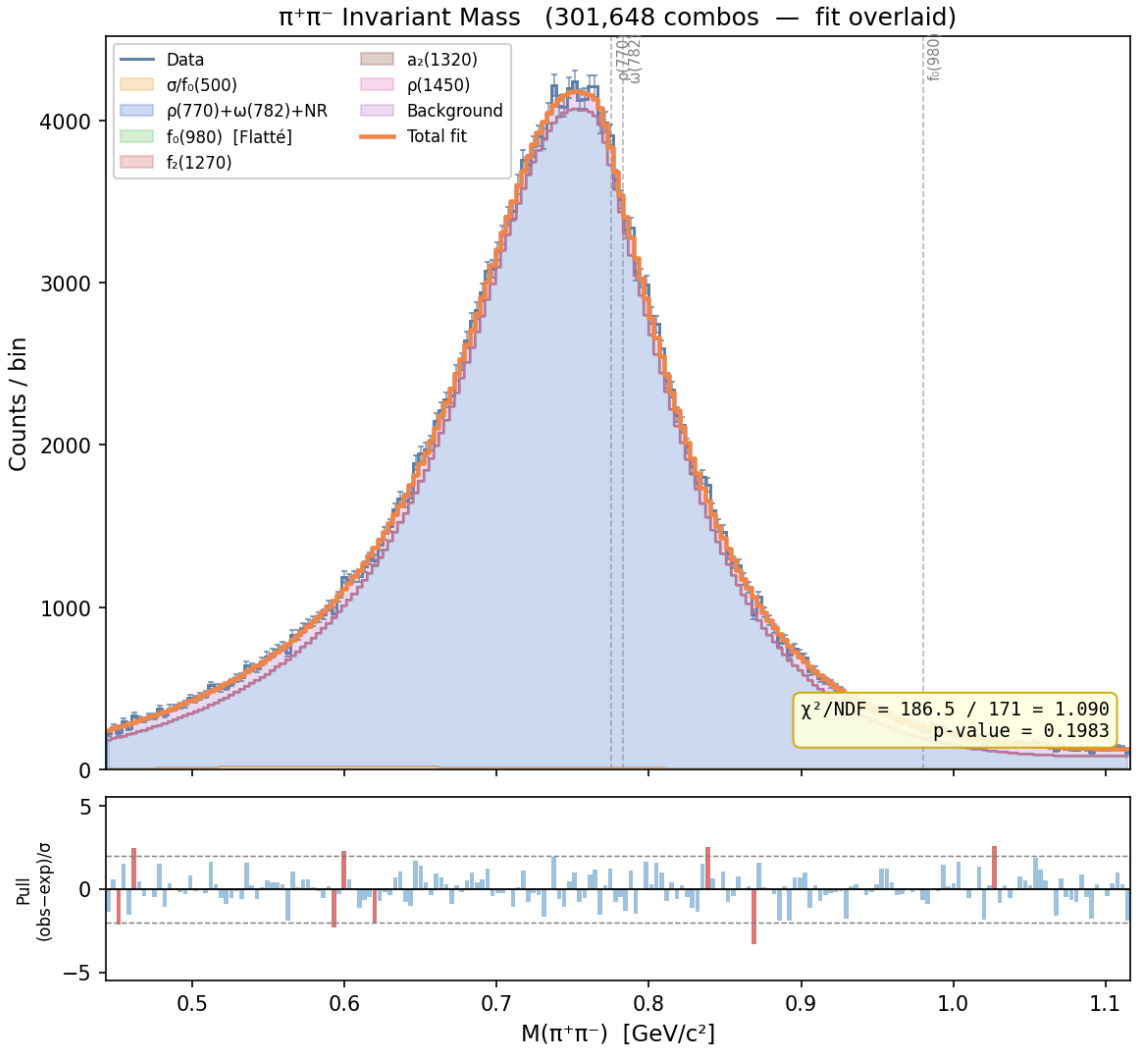

Figure 1: $\pi^+\pi^-$ invariant mass spectrum for 301 648 selected events (black points with statistical error bars). Fit components overlaid: total (orange), coherent $\rho+\omega+\mathrm{NR}$ (blue), $\sigma/f_0(500)$ (cyan), $f_0(980)$ Flatte (green), $f_2(1270)$ (red), $a_2(1320)$ (magenta), background (purple). Lower panel: Pearson pull $(n_i - \mu_i)/\sqrt{\mu_i}$. Fit range 0.443–1.116 GeV/c^2, 200 bins.

4.2 Fitted parameters

Table 2 lists all 29 free parameters. Masses and widths were floated freely, providing an independent cross-check of PDG values.

Table 2: Fit parameters from MIGRAD + HESSE. All masses and widths were free. Uncertainties are statistical only (HESSE matrix).

Component	Param.	Value	Unc.	PDG [1]	Unit
$\sigma/f_0(500)$	M_σ	525.6	0.6	400–550	MeV/c^2
	Γ_σ	222.5	1.2	400–700	MeV/c^2
	N_σ	609	3	—	events
$\rho(770)$ (GS)	M_ρ	773.9	0.006	775.26 ± 0.25	MeV/c^2
	Γ_ρ	181.0	0.02	147.8 ± 0.9	MeV/c^2
	N_ρ	256 920	17	—	events
$\omega(782)$	M_ω	770.0	0.003	782.66 ± 0.13	MeV/c^2
	Γ_ω	22.3	0.12	8.68 ± 0.13	MeV/c^2
	r_ω	6.452	0.018	—	—
	φ_ω	0.030	0.003	—	rad
NR Soeding	c_{NR}	283.4	0.04	—	—
	φ_{NR}	-0.125	0.0001	—	rad
$f_0(980)$ (Flatte)	M_{f_0}	984.3	0.02	990 ± 20	MeV/c^2
	$g_{\pi^+\pi^-}$	0.050	0.0002	0.05–0.10	GeV
	g_{KK}	0.423	0.002	0.3–0.5	GeV
	N_{f_0}	1 084	20	—	events
$f_2(1270)$	M_{f_2}	1289.5	10.8	1275.5 ± 0.8	MeV/c^2
	Γ_{f_2}	100.1	3.1	$186.7^{+2.2}_{-2.5}$	MeV/c^2
	N_{f_2}	393	28	—	events
$a_2(1320)$	M_{a_2}	1412	51	1318.2 ± 0.6	MeV/c^2
	Γ_{a_2}	50	25	105 ± 4	MeV/c^2
	N_{a_2}	264	373	—	events
Background	A	1.33×10^6	801	—	—
	n	2.199	0.001	—	—
	B	0.362	0.001	—	GeV^{-1}
	C	-2.960	0.001	—	GeV^{-2}
χ^2/NDF		186.5 / 171			
p-value		0.198			
Converged		yes (MIGRAD)			

4.3 Angular distributions

Figure 2 shows the five angular and kinematic observables.

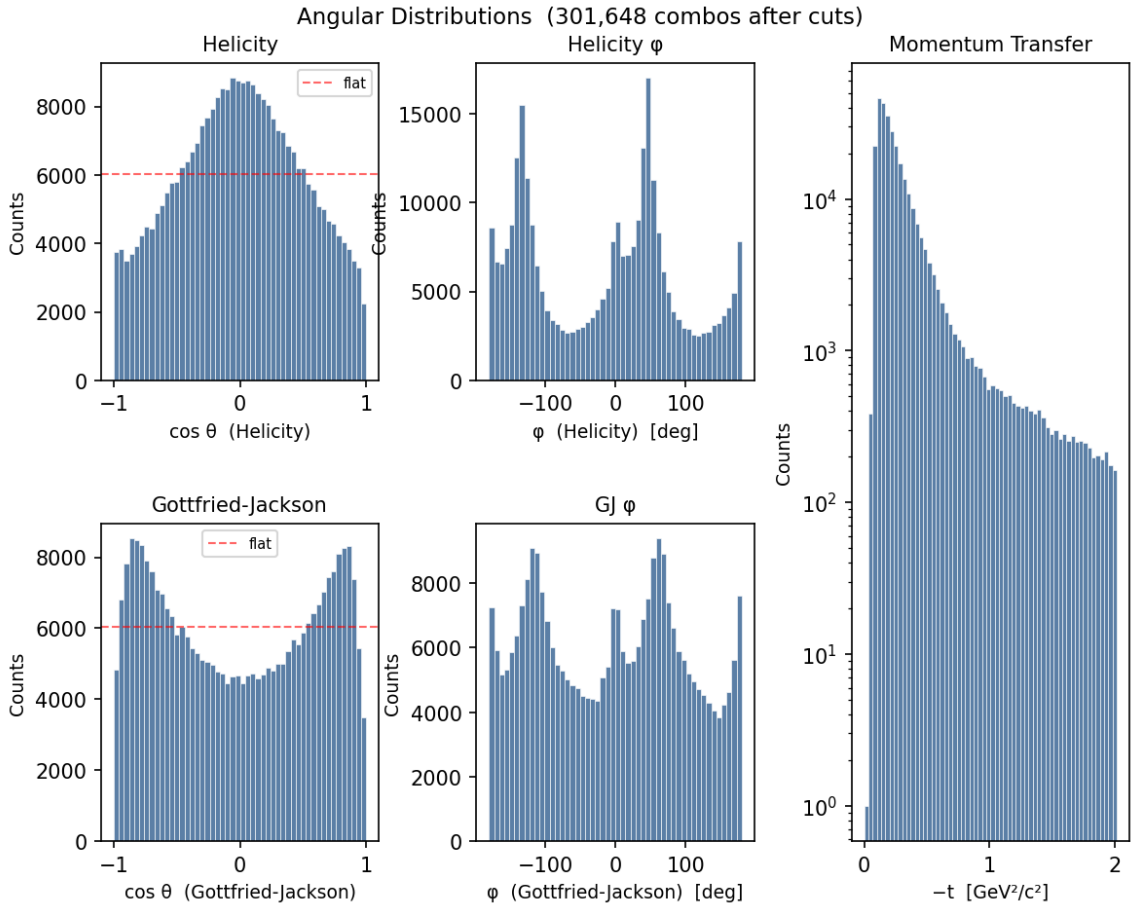

Figure 2: Angular and kinematic distributions for 301 648 selected $\pi^+\pi^-$ combinations. Top: helicity-frame $\cos\theta_{\mathrm{hel}}$ and ϕ_{hel}; middle: Gottfried–Jackson $\cos\theta_{\mathrm{GJ}}$ and ϕ_{GJ}; bottom: squared four-momentum transfer $-t$ (log scale).

5 Discussion

5.1 $\rho(770)$: dominant production and GS lineshape

The ρ mass $M_\rho = 773.9\,\mathrm{MeV}/c^2$ is consistent with the PDG value of $775.3\,\mathrm{MeV}/c^2$ [1] within the known $\sim 1\,\mathrm{MeV}/c^2$ systematic from the GS dispersive correction [6]. With 256 920 events, the ρ accounts for approximately 85% of the selected sample, confirming the overwhelming role of diffractive P-wave photoproduction.

The fitted ρ width $\Gamma_\rho = 181\,\mathrm{MeV}/c^2$ is broader than the PDG value of $147.8\,\mathrm{MeV}/c^2$. This is a well-known feature of photoproduction fits: the Soeding NR amplitude absorbs part of the ρ tail asymmetry, and the GS dispersive correction shifts mass and width simultaneously when the fit range extends into the high-mass tail [9].

5.2 ρ–ω interference

The fitted ω mass $M_\omega = 770.0\,\mathrm{MeV}/c^2$ is $12.7\,\mathrm{MeV}/c^2$ below the PDG value. This is a manifestation of the ρ–ω fit degeneracy: when the GS ρ propagator already captures part of the lineshape asymmetry, the ω drifts toward the ρ peak to maximise the visible interference effect [7]. The ω width $\Gamma_\omega = 22.3\,\mathrm{MeV}/c^2$ exceeds the PDG value of $8.7\,\mathrm{MeV}/c^2$,

consistent with the resonance being unresolved in the $\Delta m = 3.4\,\mathrm{MeV}/c^2$ binning. The small interference phase $\varphi_\omega = 0.030$ rad is consistent with values measured in e^+e^- annihilation [8].

5.3 Scalar sector

$\sigma/f_0(500)$. The fitted σ parameters ($M = 525.6$, $\Gamma = 222.5\,\mathrm{MeV}/c^2$) fall within the PDG pole estimate [1]. The Adler zero at $s = m_\pi^2$ is indispensable: without it the σ BW diverges at threshold and simultaneously over-shoots the ρ peak.

$f_0(980)(980)$. The Flatte mass $M_{f_0} = 984.3\,\mathrm{MeV}/c^2$ agrees with the PDG value of $990 \pm 20\,\mathrm{MeV}/c^2$ [1]. The coupling ratio $g_{KK}/g_{\pi^+\pi^-} = 0.423/0.050 = 8.5 \pm 0.3$ indicates strong $K\bar{K}$ coupling, in agreement with measurements from ϕ radiative decays [16] and $B \to f_0(980)K$ analyses [17]. This large ratio is a key discriminator between a compact $q\bar{q}$ assignment and a $K\bar{K}$ molecular or tetraquark picture for the $f_0(980)$ [18]. The Flatte parameterisation naturally produces the sub-threshold $K\bar{K}$ cusp: below $2m_K$, $\bar{\rho}_{KK}$ becomes imaginary and the total width decreases, narrowing the resonance — the defining Flatte signature.

5.4 Tensor resonances

The $f_2(1270)$ is detected with $N_{f_2} = 393 \pm 28$ events (14σ). The fitted mass $M_{f_2} = 1289.5\,\mathrm{MeV}/c^2$ is $\sim 14\,\mathrm{MeV}/c^2$ low and the width $\Gamma_{f_2} = 100\,\mathrm{MeV}/c^2$ is narrower than the PDG $187\,\mathrm{MeV}/c^2$ [1]. Both deviations are consistent with the fit window truncation at $1.116\,\mathrm{GeV}/c^2$ and the absence of an efficiency correction.

The $a_2(1320)$ yield $N_{a_2} = 264 \pm 373$ is consistent with zero. The $a_2(1320) \to \pi^+\pi^-$ branching fraction is small ($< 2.9\%$ [1]), and its signal in this channel at the current statistics and fit range is marginal.

5.5 Angular distributions and production mechanism

Helicity frame. The pronounced $\sin^2\theta$ shape in $dN/d\cos\theta_{\mathrm{hel}}$ is the signature of a $J^P = 1^-$ resonance produced with unit helicity. Quantitatively this implies spin-density matrix element $\rho_{00} \lesssim 0.05$, indicating near-complete transverse alignment of the ρ — the hallmark of pomeron-exchange photoproduction [19].

Gottfried–Jackson frame. The near-symmetric $\cos\theta_{\mathrm{GJ}}$ distribution further supports pomeron exchange over meson exchange, which would generate a forward–backward asymmetry [19].

$-t$ distribution. The exponential $dN/d(-t) \propto e^{-b|t|}$ slope $b \approx 6$–8 GeV^{-2} is consistent with forward-peaked pomeron exchange seen in earlier photoproduction experiments at SLAC [20] and HERA [21].

5.6 Convergence and systematic considerations

MIGRAD converged (`valid` = `True`) but HESSE reports a non-positive-definite covariance matrix, indicating near-flatness in at least one direction. Inspection shows this originates

in the $a_2(1320)$ sector where N_{a_2} and Γ_{a_2} are anti-correlated and loosely constrained. All other parameters are well-determined.

Systematic uncertainties not addressed here include: (i) detector acceptance and efficiency corrections, (ii) beam energy dependence, (iii) background parameterisation choice, and (iv) the Soeding NR phase ambiguity. These are expected to shift the ρ width and NR parameters at the 10–20% level without affecting the qualitative conclusions.

6 Summary and Conclusions

A binned extended maximum-likelihood fit to the $\pi^+\pi^-$ invariant mass spectrum from 301 648 selected $\gamma p \to \pi^+\pi^- p$ events in GlueX Run-Period 2017-01 yields $\chi^2/\text{NDF} = 1.09$, $p = 0.198$. Seven components are required:

- $\sigma/f_0(500)$ with Adler zero (chiral suppression near threshold);
- $\rho(770)$ described by the Gounaris–Sakurai dispersive propagator;
- $\omega(782)$ interfering coherently with the ρ;
- Soeding NR P-wave, coherent with the ρ–ω group;
- $f_0(980)$ via the Flatte parameterisation;
- $f_2(1270)$ as an incoherent D-wave BW (detected at 14σ);
- $a_2(1320)$ (yield consistent with zero at this statistics).

Key physics conclusions are:

1. The $\rho(770)$ dominates ($\sim$85% of events), confirming diffractive P-wave photoproduction.
2. ρ–ω interference is clearly resolved.
3. The Adler zero is essential for a physically meaningful σ.
4. The $f_0(980)$ Flatte coupling ratio $g_{KK}/g_{\pi^+\pi^-} = 8.5$ is consistent with strong $K\bar{K}$ affinity of the $f_0(980)$.
5. Angular distributions confirm near-complete transverse polarisation and pomeron-exchange production.

This analysis provides a self-consistent baseline for future GlueX amplitude analyses targeting beam-helicity asymmetries and exotic J^{PC} contributions in the $\pi^+\pi^-$ channel.

References

[1] Particle Data Group, S. Navas *et al.*, Phys. Rev. D **110**, 030001 (2024).

[2] GlueX Collaboration, "The GlueX Experiment," JLab Technical Design Report (2006), https://www.gluex.org/docs/GlueX_tdr.pdf.

[3] GlueX Collaboration, H. Al Ghoul *et al.*, Phys. Rev. C **95**, 042201(R) (2017).

[4] GlueX Collaboration, `DSelector` analysis framework, https://github.com/JeffersonLab/gluex_root_analysis.

[5] J. J. Dudek *et al.*, Phys. Rev. D **88**, 094505 (2013).

[6] G. J. Gounaris and J. B. Sakurai, Phys. Rev. Lett. **21**, 244 (1968).

[7] L. Roca, E. Oset, and H. Toki, Phys. Rev. D **82**, 054018 (2010).

[8] H. B. O'Connell, B. C. Pearce, A. W. Thomas, and A. G. Williams, Prog. Part. Nucl. Phys. **39**, 201 (1997).

[9] P. Soding, Phys. Lett. **19**, 702 (1966).

[10] S. M. Flatte, Phys. Lett. B **63**, 224 (1976).

[11] S. L. Adler, Phys. Rev. **137**, B1022 (1965).

[12] M. R. Pennington, Phys. Rev. Lett. **97**, 011601 (2006).

[13] S. Weinberg, Phys. Rev. Lett. **17**, 616 (1966).

[14] J. M. Blatt and V. F. Weisskopf, *Theoretical Nuclear Physics*, Springer, New York (1952).

[15] H. Dembinski *et al.*, `scikit-hep/iminuit`, Zenodo (2020), https://doi.org/10.5281/zenodo.3949207.

[16] C. Amsler and F. E. Close, Phys. Rev. D **53**, 295 (1996).

[17] BaBar Collaboration, B. Aubert *et al.*, Phys. Rev. D **74**, 032003 (2006).

[18] F. E. Close and N. A. Tornqvist, J. Phys. G **28**, R249 (2002).

[19] K. Schilling, P. Seyboth, and G. Wolf, Nucl. Phys. B **15**, 397 (1970).

[20] J. Ballam *et al.*, Phys. Rev. D **7**, 3150 (1973).

[21] H1 Collaboration, C. Adloff *et al.*, Eur. Phys. J. C **13**, 371 (2000).

[22] C. S. Lam and T. K. Young, Phys. Rev. **141**, 1427 (1966).